

Martensite's Logistic Paradigm

José Roberto Costa Guimarães^a, Paulo Rangel Rios^a , André Luiz Moraes Alves^{b*} 

^aUniversidade Federal Fluminense, Escola de Engenharia Industrial Metalúrgica de Volta Redonda, Av. dos Trabalhadores, 420, 27255-125, Volta Redonda, RJ, Brasil

^bUniversidade Federal do Rio de Janeiro, Centro de Tecnologia, Departamento de Engenharia Metalúrgica e de Materiais, Av. Horácio Macedo, 2030, Bloco F, Cidade Universitária, 21941-598, Rio de Janeiro, RJ, Brasil

Received: August 14, 2020; Revised: December 28, 2020; Accepted: April 01, 2021

This work introduces a deterministic approach to the martensite transformation curve. Martensite is a nucleation-controlled transformation that has two characteristics: autocatalysis and auto-accommodation. Only a small number of martensite units initially form owing to primary nucleation. These new units may cause the transformation of other units by autocatalysis. We call this kind of transformation chained autocatalysis. Moreover, as the transformation progresses, the auto-accommodation influences the arrangement of new units. This work assumes that the transformation-saturation relates to the exhaustion of the chained autocatalysis, which underlines the microstructure. To compare, we considered the KJMA's extended-transformation concept that implies assuming exhaustion by impingement. Data from isothermal martensite transformations and anisothermal martensite transformations are used to validate the model. Those data comprised different grain sizes and carbon contents. The model is based upon Verhulst's logistic concept. We propose that the model's high fitting-capability stems from its deterministic aspect combined with martensite's self-similarity. Additionally, we suggest that chained autocatalysis controls the rate of martensite transformation. Therefore, the relaxation of transformation strains by plasticity assisted by mutual accommodation determines the transformation's martensite volume in the absence of post-propagation coarsening/coalescence.

Keywords: Martensitic transformations, microstructure, logistic equation, analytical methods, Avrami's equation.

1. Introduction

The transformation curve, that is, the volume fraction transformed, V_V , against time, t , is a tool in research and process development and industrial operations. Modeling the transformation curve is an issue that has been studied for decades. In the late thirties and early forties of the last century, Kolmogorov, Johnson-Mehl, and Avrami¹⁻⁵, KJMA, published seminal papers on this subject. KJMA used a geometrical model to obtain transformation curves. KJMA supposed that the growing regions were spherical, that their growth rate was a constant, that the nuclei were uniform randomly located in space, and that the nucleation took place in two ways: site-saturation and constant nucleation-rate. Their most important contribution was how to consider impingement⁶. As Liu et al.⁷ put it, "KJMA's model consists of nucleation, growth, and impingement." KJMA model was generalized in different directions. One direction was to obtain more KJMA-like expressions using mathematically exact methods when nucleation and growth took place in a way distinct from KJMA's. Recently, Rios and Villa⁸ used mathematical methods for this purpose. The disadvantage of such an approach is that a limited number of situations admit an exact expression. Another possibility, suggested

by Avrami herself, is to employ the well-known "Avrami's equation," which is an expression containing two adjustable parameters: k and n

$$V_V = 1 - \exp(-kt^n) \quad (1)$$

Focusing the transformations in steels, the present authors have proposed an alternative to Avrami's equation⁹⁻¹¹

$$V_V = 1 - \exp\left(-V_{Vi} \left(\frac{\xi - \xi^*}{\xi_i - \xi^*}\right)^{\varphi^K}\right) \quad (2)$$

In the equation above, ξ is an "advance" variable, which in previous works⁹⁻¹¹ was equal to temperature, magnetic field, mechanical deformation, and time. The ξ_i is the first datum in a dataset. V_{Vi} is the integration constant resulting from the process of obtaining Equation 2. We denote this as V_{Vi} . This constant is a small volume fraction transformed when the martensite transformation starts. In this work, one uses V_{Vi} as a fitting parameter. ξ^* and φ^K are also fitting parameters. Throughout the text, one discusses the meaning of these parameters. This equation showed excellent agreement when fitted to transformations ranging from martensite to pearlite^{10,11}.

*e-mail: andrealves@metalmat.ufrrj.br

However, another way to approach formal kinetics is possible. Abramov's idea¹² of using Verhulst's logistic equation¹³ as the basis to describe transformation kinetics represents a significant shift of paradigm. For the derivation of the transformation curve, the kinetic ideas *are expressed directly by mathematics* instead of mediated by the transformation's geometry, as did KJMA. The purpose of using such an approach for modeling transformations is not new. In 1938, Austin and Rickett¹⁴ took the logistic equation as their starting point to obtain the so-called "Austin-Rickett equation":

$$\frac{V_V}{1-V_V} = kt^n \quad (3)$$

In 1938 not all KJMA's papers had already been published. The so-called Austin-Rickett equation is seldom applied today, superseded by KJMA's developments.

The description/rationalization of the fundamental aspects of martensite transformations¹⁵⁻²⁰ constructed the present understanding of martensite. That is, the martensite is a diffusionless and nucleation-controlled transformation. This understanding has been a particular venue to develop steels with optimized characteristics to suit the engineering demand. Martensite bears a lattice-correspondence with the austenite matrix. It also possesses a notable shape-change whose relaxation influences the geometric aspects of its constricted microstructure. Moreover, martensite-units do not coarsen or coalesce after propagation.

Consequently, the austenite grains confine the transformation because impingement on high-angle boundaries disassembles the reaction mechanism. However, martensite impingement on the grain-boundaries raises a stress field that can stimulate further intragrain and intergrain transformations to optimize transformation strains' accommodation. Thus, the first units can induce the formation of other units through autocatalysis. We call this kind of transformation chained autocatalysis. Chained autocatalysis occurs after the initial heterogeneous nucleation events in a scarce number of randomly scattered austenite grains²⁰.

2. Verhulst's Logistic Equation

The nucleation-controlled aspect of the martensite transformation is compatible with the original Verhulst equation¹³. Verhulst analyzed the sustainability of population-growth based on his "logistic equation"

$$\frac{dN(t)}{dt} = \dot{r} \cdot N(t) \cdot \left(1 - \frac{N(t)}{N_{MAX}}\right) \quad (4)$$

where $N(t)$ means the population, t means the time, \dot{r} stands for the population-intrinsic growth-rate and N_{MAX} stands for the maximum population, which can be maintained by available resources. Thus, Equation 4 is consistent with martensite's autocatalytic kinetic. Equation 4 also agrees with the view that the transformation process may be studied in terms of propagation-events since the transformation is nucleation-controlled, and the martensite units do not grow/coalesce after propagation. Furthermore, Equation 4 implies that the transformation-saturation is determined by nucleation-exhaustion instead of the matrix's volumetric exhaustion. Indeed, experimental results show that saturation

may occur for a volume fraction transformed $V_V \ll 1$ ^{21,22}. Therefore assuming that post-incubation autocatalysis controls the transformation, we substituted $\dot{r} = \varphi(\Delta)/t$, where $\varphi(\Delta)$ is a time-independent transformation-intrinsic factor referred to the external *process variable*, Δ , e.g., driving force, temperature, or an applied field. This substitution is equivalent to admitting the pertinence of self-similarity²³. Besides, both the morphology and the auto-accommodated of the martensite units suggest self-similarity. See Figure 1 in ref²⁴. Thus, we recast Equation 4 to describe the martensite transformation curves,

$$\frac{dN_V(\xi)}{d(\xi - \xi^*)} = \varphi(\Delta) \cdot \frac{N_V(\xi)}{(\xi - \xi^*)} \cdot \left(1 - \frac{N_V(\xi)}{N_{VMAX}}\right) \quad (5)$$

where ξ is the experimental "advance" variable and the subscript "V" indicates per unit volume of material, ξ^* is the incubation delay. Since we cannot calculate ξ^* or $\varphi(\Delta)$ from first principles, they are treated here as fitting parameters.

Then, acknowledging that transformation curves are usually described in terms of the fraction transformed, V_V , we recall $N_V(\xi) = V_V(\xi) / \bar{v}_{N_V}(\xi)$ where $\bar{v}_{N_V}(\xi)$ is the mean volume of the martensite units. We calculate $N_{VMAX} = 1 / \bar{v}_{N_{VMAX}}$. Introducing these relationships into Equation 5 includes the influence of the relaxation of the transformation strains, which affects the growth of the martensite units, into the logistic model. The $\varphi(\Delta)$ refers to this crucial process,

$$\frac{dV_V(\xi)}{V_V(\xi) \cdot A(V_V(\xi))} = \varphi(\Delta) \cdot \frac{d(\xi - \xi^*)}{\xi - \xi^*} \quad (6)$$

where $A(V_V(\xi)) = 1 - \left(\frac{\bar{v}_{N_{VMAX}}}{\bar{v}_{N_V}(\xi)}\right) V_V(\xi)$. Equation 6 can be integrated by separation, however an exact expression for $A(V_V(\xi))$ is not available. Thus, we considered two approximations. The invariance of the mean martensite units proposed by Magee²⁵ and the KJMA's approach assumes transformation in extended space¹⁻⁵. In the first case $A(V_V(\xi)) = 1 - V_V(\xi)$, so that the integration of Equation 6 yields a formal analog of the "Austin-Rickett equation,"

$$\frac{V_V(\xi)}{1-V_V(\xi)} = V_V(\xi_i^*) \left(\frac{\xi - \xi^*}{\xi_i - \xi^*}\right)^{\varphi(\Delta)} \quad (7)$$

where ξ_i refers to the value of ξ at the beginning of the transformation detected in the experimental dataset. We suppose $V_V(\xi_i) \ll 1$, what is reasonable in the absence of an initial transformation-burst. To use KJMA's impingement-correction, we set $A(V_V(\xi)) = 1$ and substitute the extended-volume fraction transformed, $V_{VE}(\xi)$, for $V_V(\xi)$ into Equation 6, where subscript "E" signals "extended." The integration of Equation 6 in extended space yields

$$V_{VE}(\xi) = V_{VE}(\xi_i^*) \left(\frac{\xi - \xi^*}{\xi_i - \xi^*}\right)^{\varphi(\Delta)} \quad (8)$$

Then, using KJMA's well-known equation, $V_V = 1 - \exp(-V_{VE}(\xi))$, one also obtains

$$V_V(\xi) = 1 - \exp\left(-V_V(\xi^*) \left(\frac{\xi - \xi^*}{\xi_i - \xi^*}\right)^{\varphi(\Delta)}\right) \quad (9)$$

that is analog to Equation 2.

Summing up, we have obtained two logistic equations where autocatalytic nucleation advances the transformation, but the volume fraction transformed depends on the relaxation of the transformation strains. Noteworthy the parameter $\varphi(\Delta)$ refers to the relaxation of the transformation strains which influences the growth of the martensite units, whereas the transformation exhaustion described by $A(V_V(\xi))$ depends on the arrangement of the martensite in the austenite grains and the spread of the transformation over the austenite grains²⁶.

3. Experimental Data

As in the previous work, we imported databases from papers found in peer-reviewed scientific journals to validate

the proposed equations. To fit the analytical expression to the experimental values, one calculated the sum-of-squares, ΣSQ , between experimental and calculated values of $V_V(\xi)$. The ΣSQ gives a "global" idea of the fitting quality. One may also define the relative distance, δ , between the experimental data and the analytical solution predictions

$$\delta(\%) = \frac{|V_{VEXP}(x) - V_{VA}(x)|}{V_{VEXP}(x)} \times 100 \quad (10)$$

where $V_{VEXP}(x)$ means volume fraction imported from experimental data and the $V_{VA}(x)$ means the volume fraction predicted by the analytical equations. As already established, experimental procedures may be subject to errors. One can consider a reasonable error of 5% for metallurgical experiments. Regarding the error of 5%, Tables 1-5 show the percentage of the number of points below the error of 5%. This number can help to give a quantitative basis for the fitting besides ΣSQ and visual inspection.

4. Isothermal Transformation

Table 1. Fitting Parameters - FeNiMn - Isothermal Martensite.

T, K	Equation 11 Logistic					Equation 12 KJMA				
	$\varphi(T)$	V_{Vi}	τ, s	ΣSQ	$\delta < 5\%$	$\varphi(T)$	V_{Vi}	τ, s	ΣSQ	$\delta < 5\%$
77	2.8	2.3×10^{-3}	2.8×10^2	6.6×10^{-4}	79.8%	1.7	8.1×10^{-9}	6.9×10^2	4.6×10^{-3}	58.3%
133	1.7	6.4×10^{-4}	2.4×10^2	1.5×10^{-2}	71.4%	0.9	6.8×10^{-5}	2.6×10^2	4.1×10^{-2}	53.6%
143	1.5	5.5×10^{-3}	1.7×10^2	1.5×10^{-2}	75.0%	0.7	2.7×10^{-4}	1.7×10^2	6.8×10^{-2}	61.9%
163	1.3	1.1×10^{-3}	7.5×10^1	4.9×10^{-2}	72.6%	0.5	5.8×10^{-3}	7.6×10^1	1.0×10^{-1}	65.5%
173	1.5	3.3×10^{-4}	7.5×10^1	4.7×10^{-2}	72.8%	0.7	3.6×10^{-4}	7.7×10^1	1.0×10^{-1}	66.7%
193	2.5	2.1×10^{-3}	1.9×10^2	8.5×10^{-4}	35.7%	2.6	1.5×10^{-12}	1.9×10^3	2.6×10^{-3}	19.6%
203	2.6	4.9×10^{-3}	3.4×10^2	3.3×10^{-5}	54.1%	2.8	2.5×10^{-12}	3.4×10^3	3.2×10^{-5}	54.1%

Table 2. Fitting Parameters - FeCrNi maraging steel - Isothermal Martensite.

Field (kOe)	Equation 11 Logistic					Equation 12 KJMA				
	$\varphi(T)$	V_{Vi}	τ, s	ΣSQ	$\delta < 5\%$	$\varphi(T)$	V_{Vi}	τ, s	ΣSQ	$\delta < 5\%$
0	3.5	2.0×10^{-8}	1.2×10^4	9.5×10^{-5}	75.0	2.8	4.0×10^{-7}	1.2×10^4	5.5×10^{-5}	100.0
20	2.7	3.2×10^{-5}	9.3×10^2	5.7×10^{-5}	95.5	1.9	1.6×10^{-5}	1.3×10^3	2.7×10^{-4}	72.7
40	2.1	1.3×10^{-3}	7.6×10^2	1.0×10^{-4}	100.0	1.4	4.7×10^{-4}	1.2×10^3	2.2×10^{-4}	72.2
60	2.1	2.5×10^{-6}	2.8×10^2	2.4×10^{-4}	75.0	1.6	1.1×10^{-4}	2.7×10^2	5.2×10^{-5}	100.0
90	1.7	2.5×10^{-4}	3.3×10^2	6.7×10^{-4}	60.9	1.4	1.3×10^{-3}	3.2×10^2	7.2×10^{-5}	95.7

Table 3. Fitting Parameters - FeMnSiMo - Athermal Martensite.

D, mm	T_i, K	Equation 14 Logistic					Equation 15 KJMA				
		$\bar{\varphi}_G$	V_{Vi}	T^*, K	ΣSQ	$\delta < 5\%$	$\bar{\varphi}_G$	V_{Vi}	T^*, K	ΣSQ	$\delta < 5\%$
0.185	628	4.0	2.3×10^{-3}	646.6	3.5×10^{-2}	83.3%	1.4	2.8×10^{-4}	628.1	4.9×10^{-2}	69.7%
0.067	628	3.1	4.5×10^{-4}	643.5	8.9×10^{-3}	87.7%	1.3	7.1×10^{-4}	623.1	8.1×10^{-2}	58.5%
0.025	638	3.6	4.5×10^{-5}	643.5	1.8×10^{-2}	79.4%	1.3	5.3×10^{-4}	613.1	1.1×10^{-1}	39.7%
0.015	608	2.7	2.2×10^{-3}	613.2	2.4×10^{-2}	88.7%	1.0	7.0×10^{-4}	607.8	1.2×10^{-1}	59.7%
0.006	608	3.3	6.3×10^{-4}	613.2	1.2×10^{-2}	83.6%	1.4	4.5×10^{-5}	607.8	1.7×10^{-1}	47.5%

Table 4. Fitting Parameters - FeCrNi - Athermal Martensite.

wt%C	T_i , K	Equation 14 Logistic					Equation 15 KJMA				
		$\bar{\varphi}_G$	V_{Vi}	T^* , K	ΣSQ	$\delta < 5\%$	$\bar{\varphi}_G$	V_{Vi}	T^* , K	ΣSQ	$\delta < 5\%$
0.002	290	3.7	1.2×10^{-1}	339.7	7.0×10^{-4}	88.9	1.3	8.6×10^{-2}	299.2	8.1×10^{-4}	93.3
0.020	265	4.0	3.7×10^{-2}	304.7	3.6×10^{-4}	96.9	1.5	6.4×10^{-3}	267.8	8.8×10^{-4}	96.9
0.050	254	5.5	1.2×10^{-2}	304.1	2.3×10^{-4}	88.9	2.4	8.0×10^{-3}	265.4	4.1×10^{-4}	77.8
0.100	193	6.1	4.6×10^{-2}	242.6	1.1×10^{-4}	90.0	2.8	6.6×10^{-2}	218.4	3.2×10^{-5}	90.0

Table 5. Fitting Parameters - Carbon Steels - Athermal Martensite.

wt%C	T_i , K	Equation 14 Logistic					Equation 15 KJMA				
		$\bar{\varphi}_G$	V_{Vi}	T^* , K	ΣSQ	$\delta < 5\%$	$\bar{\varphi}_G$	V_{Vi}	T^* , K	ΣSQ	$\delta < 5\%$
0.46	586	1.8	1.7×10^{-3}	587.5	3.0×10^{-2}	65.1%	1.0	8.7×10^{-4}	586.3	8.5×10^{-2}	49.2%
0.66	535	2.3	1.6×10^{-2}	546.0	1.6×10^{-2}	69.7%	1.2	2.9×10^{-3}	535.9	4.0×10^{-2}	53.0%
0.80	502	2.2	1.6×10^{-2}	513.9	6.3×10^{-3}	84.2%	1.2	7.9×10^{-3}	503.8	2.3×10^{-2}	52.6%

For isothermal martensite transformation, one replaces time for the advancing variable in the equations of the previous section, so Equation 7 becomes

$$\frac{V_V(t)}{1-V_V(t)} = V_{Vi} \left(\frac{t-\tau}{t_i-\tau} \right)^{\varphi(T)} \quad (11)$$

and Equation 9 becomes

$$V_V(t) = 1 - \exp \left(-V_{Vi} \left(\frac{t-\tau}{t_i-\tau} \right)^{\varphi(T)} \right) \quad (12)$$

where τ is the incubation time, t_i is the first transformation-time datum of the dataset, and T means the temperature. The isothermal-martensite database, Fe-23.2wt%Ni, 2.8wt%Mn, 0.009wt%C, grain intercept 0.048 mm, was initially described in ref²². The isothermal-martensite database, Fe-12wt%Cr, 9wt%Ni maraging steel, was presented in ref²⁷. Since the imported data did not allow a precise determination of the incubation time, we assumed $\tau = \lambda \cdot t_i$, and fitted λ until the sum-of-squares, ΣSQ , between experimental and calculated values of V_V , became invariant. The values of the fitting parameters in Equations 11 and 12: τ , V_{Vi} , and $\varphi(T)$ along with the respective values of ΣSQ , are shown in Tables 1 and 2. Figure 1 shows the FeNiMn database as-fitted. Figure 2 shows the maraging curves as-fitted.

The values of ΣSQ point out that Equation 11 performed slightly better than Equation 12. Visual inspection is consistent with ΣSQ values. That is, both expressions provided a good fit despite their different formal-approaches to transformation-saturation. The behavior of the parameter δ confirms this.

Concentrating on the FeNiMn alloy, Table 1 and Figures 3 and 4, at the high transformation temperatures, $\varphi(T)$ refers to a thermally activated process. By contrast, at the lower temperatures, 163K - 77K, the anti-thermal variation in $\varphi(T)$ points to the mechanical autocatalysis, which feeds back strain energy²⁸. Phenomenologically, we propose,

$$\varphi(T) = \varphi_0 \frac{\Delta Ga}{k_B T} \exp \left(-\frac{Ea}{k_B T} \right) \quad (13)$$

where φ_0 is a proportionality factor, Ea , and ΔGa are apparent energies, T is the reaction temperature and k_B is the Boltzmann constant. The charts in Figure 3 yield $Ea \approx 5$ kJ/mol - 13 kJ/mol, which is compatible with dislocation processes, and $\Delta Ga \approx 0.9$ - 1.3 kJ/mol, which has the same magnitude as the elastic free-energy (0.9 kJ/mol) of an oblate spheroid with a typical 0.05 aspect-ratio in a constrained matrix²⁹. The FeNiMn isothermal martensite undergoes a substructure change at low transformation temperatures²². Thus, we propose that the variation in $\varphi(T)$ refers to changes in the relaxation of transformation strains³⁰. The variation in the V_{Vi} corroborate the variation in $\varphi(T)$. However, the variations in $1/\tau$ show the opposite trends, see Figure 4. Such specific behavior point to differences in the martensite propagation. Martensite propagation at incubation depends on the probability that austenite defects sustain coordinated atomic groups to cross the nucleation path^{31,32}. By contrast, the nucleation's post-incubation is determined by a previously formed martensite unit (autocatalysis feedback)^{28,33}. At high-temperature thermal agitation hamper atomic groups' stability, creating an entropic barrier for converting such groups into nuclei. Thence the chemical driving force controls the incubation. Instead, at low temperatures (higher driving forces), a thermal barrier controls the martensite incubation/nucleation. In this regard, it is noteworthy that the apparent activation energy obtained from the incubation time, ~ 6 kJ/mol, compare with the ~ 5 kJ/mol obtained from the parameter $\varphi(T)$, which refers to the accommodation of the shape strain at high transformation temperatures. This comparison says that dislocation processes are present in both processes (relaxations of lattice-misfit and the shape strain). At this time, the analysis of the temperature variation in the parameter V_{Vi} was not conclusive.

Lastly, mind that impingement of martensite on the austenite grain boundary generates a stress-field capable of fostering martensite propagation into the next grain^{26,34}. However, such an "intergrain-spread" is hindered if the austenite plasticity halts the radial propagation of a martensite unit³⁵. Such a possibility is comparable to "soft-impingement."

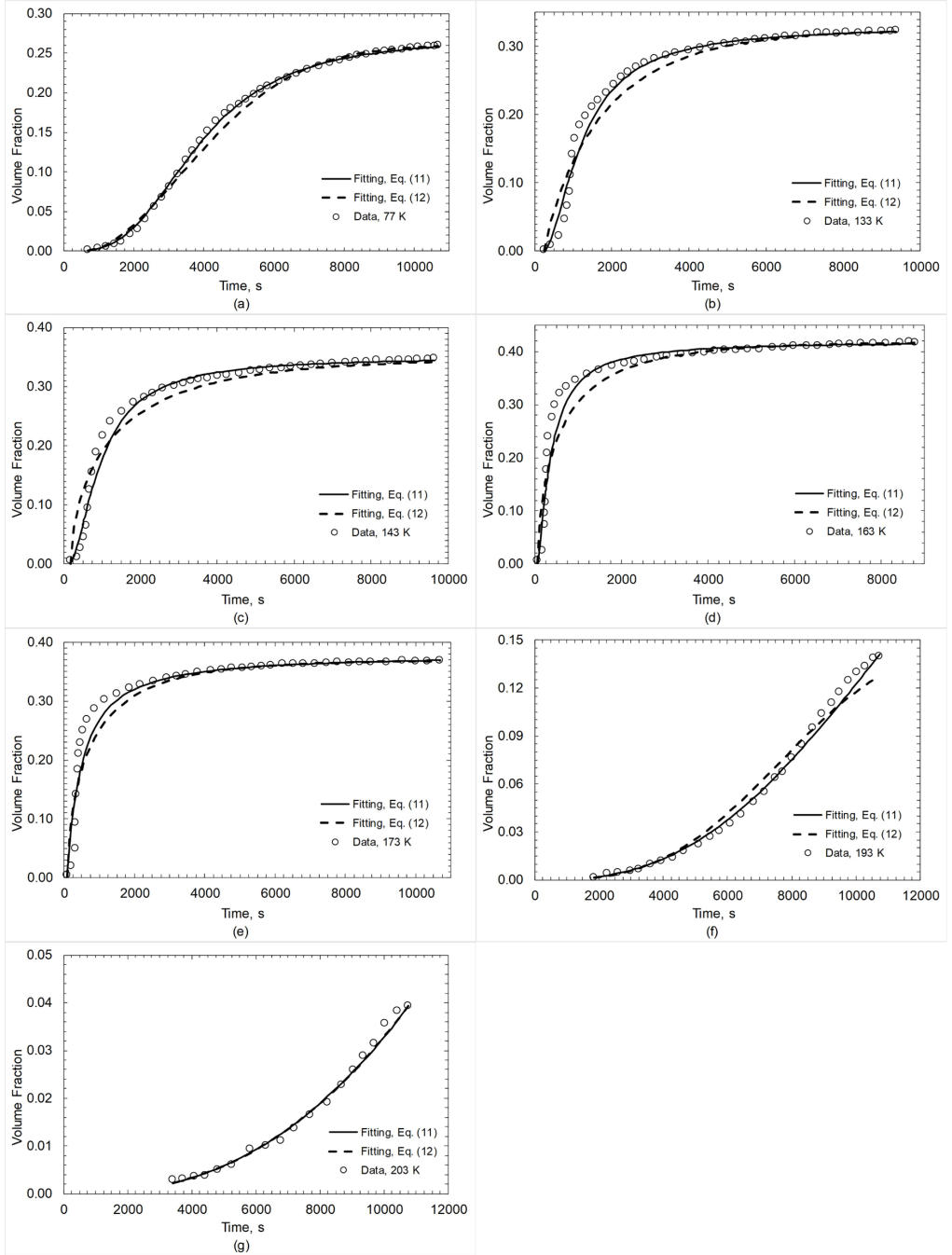


Figure 1. FeNiMn isothermal transformation for different temperatures. (a) 77 K; (b) 133 K; (c) 143 K; (d) 163 K; (e) 173 K; (f) 193 K; (g) 203 K. Data extracted from ref²². Graphs were constructed and fitted with Equations 11 and 12.

5. Martensite “Athermal” Transformation

To describe the transformation curve of time-independent, driving-force induced (“athermal”) martensite, one replaces temperature for the advancing variable in Equations 11 and 12 that gives:

$$\frac{V_V(T)}{1-V_V(T)} = V_{Vi} \left(\frac{T^* - T}{T^* - T_i} \right)^{\bar{\Phi}_G} \quad (14)$$

and

$$V_V(T) = 1 - \exp \left(-V_{Vi} \left(\frac{T^* - T}{T^* - T_i} \right)^{\bar{\Phi}_G} \right) \quad (15)$$

where T^* is the upper temperature for martensite nucleation, and T_i is the highest experimental temperature in a data set. The variables, V_{Vi} , T^* and $\bar{\Phi}_G$ are fitting parameters. We

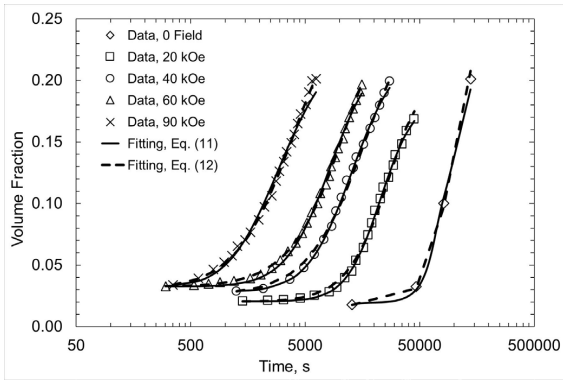


Figure 2. FeCrNi maraging steel isothermal transformation for different intensities of magnetic fields. Data extracted from ref²⁷. Graphs were constructed and fitted with Equations 11 and 12.

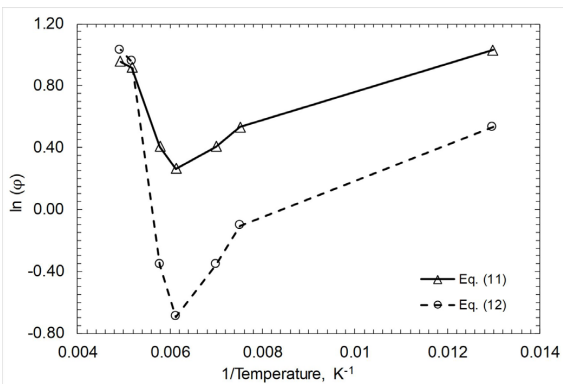


Figure 3. Arrhenius chart - Temperature variation in the parameter $\phi(T)$ obtained with Equations 11 and 12 for the FeNiMn.

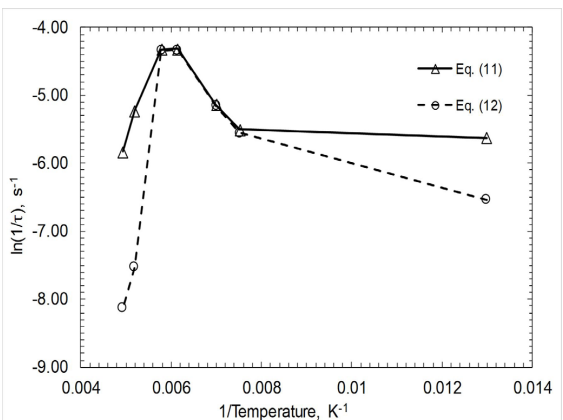


Figure 4. Arrhenius chart - Temperature variation in the incubation-time graphed as $1/\tau$ obtained with Equations 11 and 12 for the FeNiMn.

use the subscript “G” in $\bar{\varphi}_G$ to emphasize that the *driving force* is the external variable in the non-thermally activated

transformation. It is worthy of note that in the $\left(\frac{T^* - T}{T^* - T_i}\right)$ the

quantities seem to be inverted when compared with $\left(\frac{t - \tau}{t_i - \tau}\right)$.

The reason for this is that time increases and temperature decreases. Thus, the terms are inverted so that the subtractions remain positive.

Ref³⁶ describes a database typical of Fe-0.2wt%C, 3.5wt%Mn, 1.5wt%Si, 0.5wt%Mo with different grains sizes (0.006 mm - 0.185 mm). Ref³⁷ provides data on Fe-18wt%Cr, 8wt%Ni, with varying contents of carbon.

In FeMnSiMo, the transformation took place in a dilatometer. In addition to allowing the models’ validation, the database permits to characterize the austenite grain size’s influence on the transformation curve. Bearing scatter in T^* , we expressed $T^* = \lambda \cdot T_i$, and fitted λ until the sum-of-squares, ΣSQ , between experimental and calculated values of V_V became invariant, see Figure 5. Table 3 lists the values of the obtained parameters of Equations 14 and 15. Inspection of the values of ΣSQ indicates that Equation 14 provides the best fittings with a minor variation in ΣSQ . By contrast, the values of ΣSQ , which characterize the fittings with Equation 15, increase with increasing the austenite grain-size.

A similar procedure was used to fit the Fe-18wt%Cr, 8wt%Ni data. The results are shown in Figure 6 and Table 4. The fit is excellent.

Concentrating on the FeMnSiMo, Figures 7 and 8 show the values of $\bar{\varphi}_G$ and T^* graphed after Hall-Petch, complying with the experimental variable (austenite grain size). The T_i estimates the martensite start temperature, M_S . Observe that both fittings yielded decreasing values of $\bar{\varphi}_G$ and T^* with decreasing the austenite grain size down to 0.015 mm, then upshifts. The decreasing in $\bar{\varphi}_G$ suggests the influence of the austenite strength on the martensite propagation, possibly related to the mobility of the martensite-austenite interfaces or dislocation processes³⁸. The reported³⁶ coarser aspect ratio of the martensite units formed in the material with 0.006 mm grain size is coherent with a heightened variant-selection (auto-accommodation), also acknowledged in ref³⁹. The decreasing values of T^* imply higher stability in the fine-grained austenite. Thence, the variations in $\bar{\varphi}_G$ and T^* are in qualitative agreement with the conclusions in ref³⁶. The high values of ΣSQ , typical of the fittings of the dataset with Equation 15, are due to the severe effect of crystallographic-variance in fine-grain austenite. This crystallographic-variance affects the microstructure’s local-randomicity, which is a requirement for utilizing the KJMA’s methodology¹⁻⁵. Again, the behavior of the parameter δ indicated a better agreement between Equations 14 and 15, which assumes exhaustion by nucleation and by impingement, respectively.

Lastly, we consider the influence of the carbon in the martensite, transformed by continuous cooling. Typical plain carbon-steels with similar austenite grain-sizes were considered: Fe46C(0.46wt%C, 0.71wt%Mn, 0.26wt%Si, 0.1wt%Ni, 0.2wt%Cr), Fe66C(0.66wt%C, 0.69wt%Mn, 0.30wt%Si, 0.1wt%Ni, 0.2wt%Cr), and Fe80C(0.80wt%C, 0.61wt%Mn, 0.41wt%Si, 0.2wt%Ni, 0.3wt%Cr). These databases were imported from ref⁴⁰. The fittings with Equations 14 and 15 are

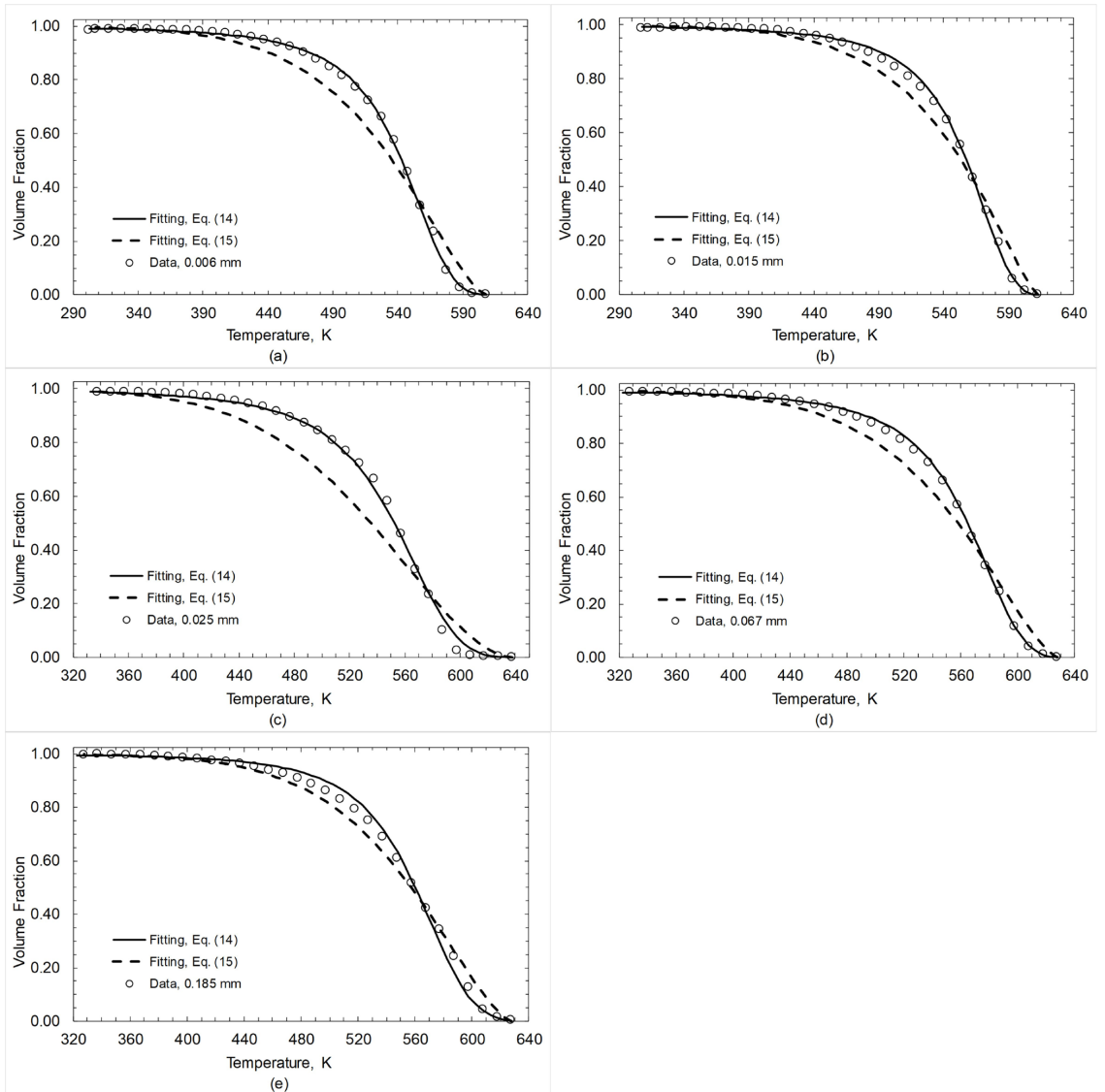


Figure 5. Comparison of fittings for the FeMnSiMo with different grains sizes, transformed by continuous cooling. (a) 0.006 mm; (b) 0.015 mm; (c) 0.025 mm; (d) 0.067 mm; (e) 0.185 mm. Data extracted from ref³⁶. Graphs were constructed and fitted with Equations 14 and 15.

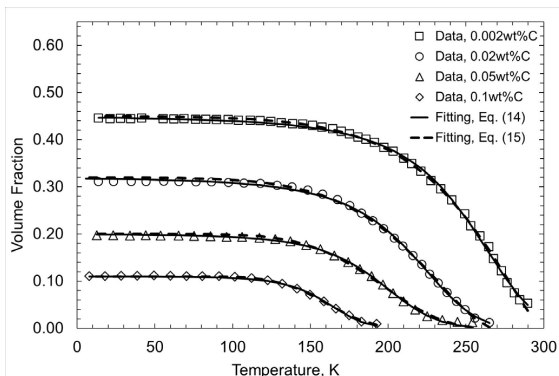


Figure 6. FeCrNi stainless steels athermal transformation during continuous cooling. Data extracted from Ref³⁷. Graphs were constructed and fitted with Equations 14 and 15.

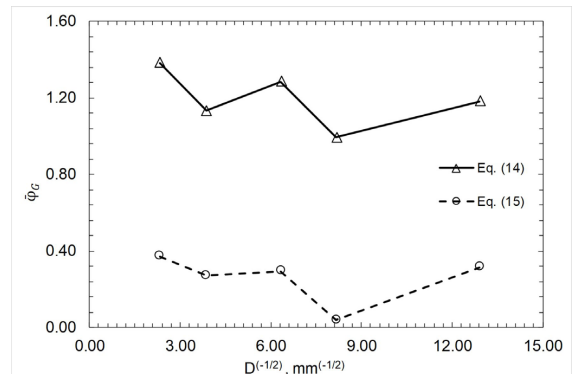


Figure 7. Values of $\bar{\Phi}_G$ graphed after Hall-Petch for the FeMnSiMo.

shown in Figure 9, and the values of the respective model-parameters are listed in Table 5. Again, visual inspections of the charts and the variations in ΣSQ indicate that the Equation 14 provided better fittings, especially concerning the transformation-charts' progressive induction. These fittings were consistent with the behavior of the parameter δ . We ascribe the variation in T^* to the influence of the carbon on the austenite stability. The variation in $\bar{\varphi}_G$ is related to the influence of carbon content on the transformation microstructure since increasing carbon enhances the partitioning of the austenite grains into finer packets and blocks⁴¹.

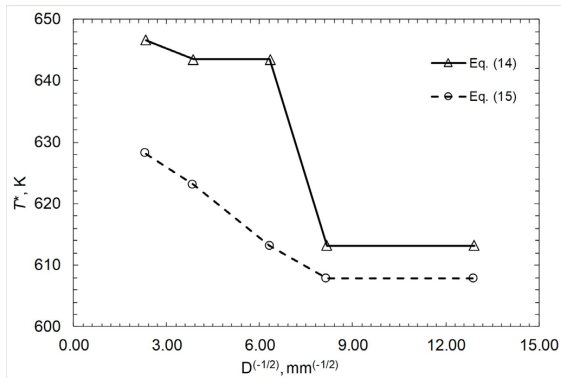


Figure 8. Values of T^* graphed after Hall-Petch for the FeMnSiMo.

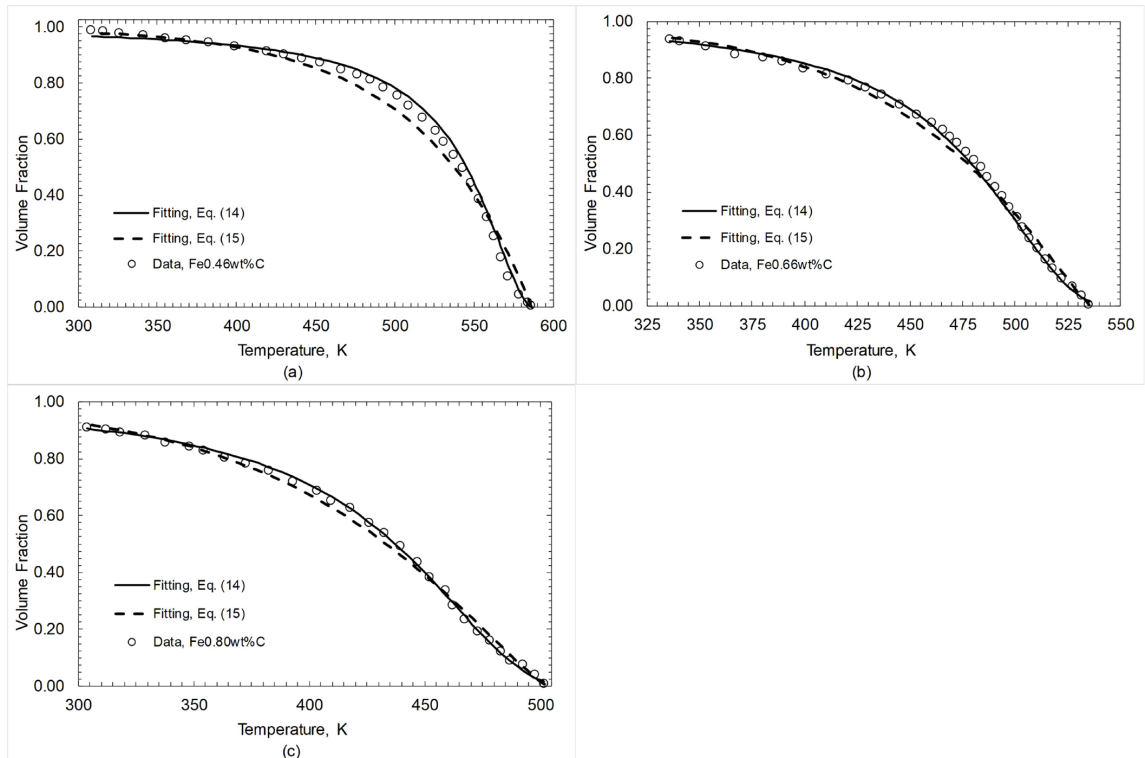


Figure 9. Martensite transformation curves of typical plain carbon-steels with similar austenite grain-sizes for different concentration of C. (a) Fe46C; (b) Fe66C; (c) Fe80C. Data extracted from ref⁴⁰. Graphs were constructed and fitted with Equations 14 and 15.

Like the isothermal transformation curves above analyzed, the different modes of considering the transformation-saturation provided proper fittings of the data. Nonetheless, the values of the fitting parameters are model-dependent, as might be expected.

6. Discussion

The classical Verhulst's logistic equation, Equation (4), proposed to describe constrained population growth, provides a venue to express transformation curves¹². Specifically, note that Equation 6 has two independent terms, $\varphi(\Delta) \cdot \frac{d(\xi - \xi^*)}{\xi - \xi^*}$ that refers to the advance of the microstructure, and $\frac{dV_V(\xi)}{V_V(\xi) \cdot A(V_V(\xi))}$ that refers to the accommodation of the transformation in the austenite grains. The integrated Equations 11 and 14 and Equations 12 and 15 only differ in the specification of the exhaustion factor, $A(V_V(\xi))$. By adjusting their fitting parameters, suitable descriptions of the transformation curves are possible.

The similar variations in the parameters $\varphi(T)$ and τ obtained with Equations 11 and 12 are coherent with the pertinence of self-similarity in the martensite transformation. Notably, the variations in the parameters obtained from the FeMnSiMo database typical of martensite transformation by cooling ("athermal") exhibit similarity and are in qualitative agreement with the results reported in the referenced paper³⁶. Thence, the experimentalists may choose the more

appropriate expression to analyze their data and describe the transformation under consideration¹². Nonetheless, the meaning of the physical parameters obtained from formal models depends on the models' premises. We assert that autocatalysis and transformation-saturation by nucleation-exhaustion are realistic premises to model martensite transformation curves as provided by Equations 11 and 14.

It is worth discussing the fitting parameters displayed in Tables 1-5.

First, we would like to offer some background on the use of phenomenological equations and fitting parameters to describe a specific kinetic curve. In the present case, to fit a $V_f(t)$ curve. The first possible approach to describe experimental measurements by an analytical expression is to employ an arbitrary function to fit the experimental curve. This fit may be useful if one has an analytical theory that takes a continuous function as its input, for example, Ref¹². On another extreme, one may fit an expression derived from fundamental theories. Generally, these are not easy to come by. An intermediary approach is to use the so-called formal kinetics. These provide exact expressions when one specifies the nucleation and growth rates. The pioneering work is, of course, KJMA theory¹⁻⁵. More recently, Rios and Villa^{8,43-45} derived several new expressions. Still, the number of exact solutions is limited.

Yet another possibility is to use functions that have some physical or mathematical basis. Such as Avrami's, see Equation 1. Or Austin-Rickett, see Equation 3. Here we used

a generalization of both Avrami and Austin-Rickett equations, containing an extra parameter related to the beginning of the transformation.

From the equation employed here, one expects: I) that they give a good fit; II) that we can extract some information from the fitting parameters. Notice that the functional form is different for Equations 14 and 15. Therefore it comes as no surprise that the absolute value of the fitting parameters differs. Nonetheless, Tables 6, 7, and 8 show that they do not differ by the same magnitude. In the case of Table 6, the differences between the fitting parameters were calculated as follows: (Equation 12 parameter – Equation 11 parameter)/(mean value of Equation 11 and Equation 12 parameters). The same reasoning was adopted for Tables 7 and 8, but with Equations 11 and 12 replaced by Equations 14 and 15.

The parameters that mark the beginning of the transformation, such as initial transformation temperature and incubation time, are physical parameters. Tables 7 and 8 demonstrates that the values of T^* lie quite close when Equations 14 and 15 determine them. Table 6 shows the values of τ , obtained from Equations 11 and 12, behave similarly but with an apparent discrepancy at the highest and lowest temperatures. The absolute values of the other parameters have a significantly higher difference. This behavior is unavoidable as the proper functions are different. This result suggests that the function

Table 6. Difference between the fitting parameters shown in Table 1 obtained by Equation 11 and Equation 12 for the FeNiMn - Isothermal Martensite.

T , K	$\varphi(T)$ Difference	V_{fi} Difference	τ Difference
77	48.9%	200.0%	-85.6%
133	61.5%	161.3%	-5.0%
143	72.7%	181.4%	-2.1%
163	88.9%	-133.9%	-2.0%
173	72.7%	-9.0%	-2.0%
193	-3.9%	200.0%	-163.6%
203	-7.4%	200.0%	-163.7%

Table 7. Difference between the fitting parameters shown in Table 3 obtained by Equation 14 and Equation 15 for the FeMnSiMo - Athermal Martensite.

D, mm	T_i , K	$\bar{\varphi}_G$ Difference	V_{fi} Difference	T^* Difference
0.185	628	96.3%	156.6%	2.9%
0.067	628	81.8%	-44.8%	3.2%
0.025	638	93.9%	-168.7%	4.8%
0.015	608	91.9%	103.4%	0.9%
0.006	608	80.8%	173.3%	0.9%

Table 8. Difference between the fitting parameters shown in Table 5 obtained by Equation 14 and Equation 15 for the Carbon Steels - Athermal Martensite.

wt%C	T_i , K	$\bar{\varphi}_G$ Difference	V_{fi} Difference	T^* Difference
0.46	586	57.1%	64.6%	0.2%
0.66	535	62.9%	138.6%	1.9%
0.80	502	58.8%	67.8%	2.0%

form of Equations 11, 12, 14 and 15 strongly influence parameters, such as, V_{Vi} and φ .

One cannot expect Equations 11, 12, 14 and 15 to be more than they are. They are equations with a physical or mathematical background, but they are still approximations. And it is well-known that fitting parameters carry the error made by assuming a certain approximation. But, as shown above, the parameters are not influenced in the same way. Here, parameters that have a direct physical interpretation tend to be almost independent of the fitting expression. By contrast, parameters that are more directly related to the functional form of the fitting expressions tend to have more considerable differences.

7. Conclusions

1. The utilization of the logistic formalism to describe isothermal and continuous cooling martensite transformations yielded quality-fittings of experimental data. These quality-fittings are consistent with current views regarding martensite's nucleation-controlled, autocatalytic kinetics, and self-similarity.
2. The apparent activation energies obtained from Equation 13, 5 kJ/mol - 13 kJ/mol, compares with the activation energies for martensite nucleation reported in refs^{46,47}. Therefore, one may suggest that there are two kinds of active dislocation processes. One dislocation process acts in the conversion of coordinated atomic groups into nuclei. The other, intrinsically different dislocation process relates to the relaxation of the martensite shape-strain³⁰.
3. The incorporation of self-similarity into Verhulst's logistic formalism allowed good descriptions of the martensite transformation curves as well as characterizations of kinetic aspects of isothermal or "athermal" transformations.

Acknowledgments

This study was financed in part by the Coordenação de Aperfeiçoamento de Pessoal de Nível Superior - Brasil (CAPES) - Finance Code 001. P. R. Rios, and A. L. M. Alves are also grateful to Conselho Nacional de Desenvolvimento Científico e Tecnológico, CNPQ, and Fundação de Amparo à Pesquisa do Estado do Rio de Janeiro, FAPERJ, for the financial support.

References

1. Kolmogorov AN. On the statistical theory of metal crystallization. *Isvetiia Acad Nauk SSSR-Seriia Mat.* 1937;1:335-59.
2. Johnson WA, Mehl RF. Reaction kinetics in processes of nucleation and growth. *Trans Metall Soc AIME.* 1939;135:416-41.
3. Avrami M. Kinetics of phase change. I: general theory. *J Chem Phys.* 1939;7(12):1103-12.
4. Avrami M. Kinetics of Phase Change II. Transformation – Time relations for random distribution of nuclei. *J Chem Phys.* 1940;8:212-24.
5. Avrami M. Granulation, Phase Change, and Microstructure Kinetics of Phase Change. III. *J Chem Phys.* 1941;9(2):177.
6. Barmak K. A Commentary on: "Reaction Kinetics in Processes of Nucleation and Growth"* . *Metall Mater Trans, A Phys Metall Mater Sci.* 2010;41(11):2711-75.
7. Liu F, Sommer F, Bos C, Mittemeijer EJ. Analysis of solid state phase transformation kinetics : models and recipes. *Int Mater Rev.* 2007;52(4):193-212.
8. Rios PR, Villa E. Transformation kinetics for inhomogeneous nucleation. *Acta Mater.* 2009;57(4):1199-208.
9. Guimarães JRC, Rios PR. Revisiting Temperature and Magnetic Effects on the Fe-30 Wt Pct Ni Martensite Transformation Curve. *Metall Mater Trans, A Phys Metall Mater Sci.* 2018;49(12):5995-6000.
10. Guimarães JRC, Rios PR. General description of martensite transformation curves—a case for bainite. *Mater Sci Technol (United Kingdom).* 2019;35(6):731-7.
11. Guimarães JRC, Rios PR, Alves ALM. An alternative to Avrami Equation. *Mater Res.* 2019;22(5):1-8.
12. Avramov I, Šesták J. Generalized kinetics of overall phase transition in terms of logistic equation. *Physics.Chem-Ph.* 2015.
13. Verhulst PF. Recherches mathématiques sur la loi d'accroissement de la population. *Nouv Mémoires L'académie R Des Sci B-lett Bruxelles.* 1845;18:1-45.
14. Austin JB, Rickett RL. Kinetics of the decomposition of austenite at constant temperature. *Am Inst Mining. Metall Pet Eng.* 1938;135:396-415.
15. Harris WJ, Cohen M. Stabilization of the austenite-martensite transformation. *Trans Metall Soc AIME.* 1949;180:447-70.
16. Fisher JC, Hollomon JH, Turnbull D. Kinetics of the austenite-martensite transformation. *Trans Metall Soc AIME.* 1949;185:691-700.
17. Bunshah RF, Mehl RF. Rate of propagation of martensite. *Trans Metall Soc AIME.* 1953;197:1251-8.
18. Wechsler MS, Lieberman DS, Read TA. On the theory of the formation of martensite. *Trans Metall Soc AIME.* 1953;197:1503-15.
19. Koistinen DP, Marburger RE. A general equation prescribing the extent of the austenite-martensite transformation in pure iron-carbon alloys and plain carbon steels. *Acta Metall.* 1959;7(1):59-60.
20. Cech RE, Turnbull D. Heterogeneous nucleation of the martensite transformation. *Trans Metall Soc AIME.* 1956;206:124-32.
21. Pati SR, Cohen M. Kinetics of isothermal martensitic transformations in an iron-nickel-manganese alloy. *Acta Metall.* 1971;19(12):1327-32.
22. Ghosh G, Raghavan V. The kinetics of isothermal martensitic transformation in an Fe-23.2wt.%Ni-2.8wt.%Mn alloy. *Mater Sci Eng A.* 1986;80(1):65-74.
23. Skrotzki B. The course of the volume fraction of martensite vs. temperature function $M_x(T)$. *Le J Phys IV.* 1991;1(C4):367-372.
24. Guimarães JRC, Rios PR. Microstructural path analysis of martensite dimensions in FeNiC and FeC alloys. *Mater Res.* 2015;18(3):595-601.
25. Magee CL. The nucleation of martensite. In: Aaronson HI, editor. *Phase transformations.* American Society for Metals; 1968. p. 115-56.
26. Guimarães JRC, Gomes JC. A metallographic study of the influence of the austenite grain size on martensite kinetics in Fe-31.9 Ni-0.02C. *Acta Metall.* 1978;26(10):1591-6.
27. Martin DS, van Dijk NH, Brück E, van der Zwaag S. The isothermal martensite formation in a maraging steel: A magnetic study. *Mater Sci Eng A.* 2008;481-482(1-2C):757-61.
28. Bokros JC, Parker ER. The mechanism of the martensite burst transformation in Fe-Ni single crystals. *Acta Metall.* 1963;11:1291-301.
29. Christian JW. Thermodynamic and Kinetics of Martensite. In: Owen WS, editor. *Proceedings of the International Conference on Martensitic Transformations, ICOMAT 1979.* Boston: ICOMAT; 1979. p. 220-34.

30. Roitburd AL. The leading role of self stress relaxation in structure and kinetic features of martensitic transformations, New Aspects of Martensitic Transformations. In: Proc First JIM International Symposium. Kobe, Japan; 1976. p. 99-103.
31. Kastner O, Shneck RZ. On the entropic nucleation barrier in a martensitic transformation. *Philos Mag.* 2015;95(12):1282-308.
32. Zhang W, Jin YM, Khachatryan AG. Phase field microelasticity modeling of heterogeneous nucleation and growth in martensitic alloys. *Acta Mater.* 2007;55(2):565-74.
33. Malik A, Yeddu HK, Amberg G, Borgenstam A, Ågren J. Three dimensional elasto-plastic phase field simulation of martensitic transformation in polycrystal. *Mater Sci Eng A.* 2012;556:221-32.
34. Raghavan V. Formation sequence of plates in isothermal martensite transformation. *Acta Metall.* 1969;17(10):1299-303.
35. Haezebrouck DM. Nucleation and growth of a single martensite particle [thesis]. Cambridge: Massachusetts Institute of Technology; 1987.
36. Celada-Casero C, Sietsma J, Santofimia MJ. The role of the austenite grain size in the martensitic transformation in low carbon steels. *Mater Des.* 2019;167:1-11.
37. Masumura T, Tsuchiyama T, Takaki S, Koyano T, Adachi K. Difference between carbon and nitrogen in thermal stability of metastable 18%Cr-8%Ni austenite. *Scr Mater.* 2018;154:8-11.
38. Olson GB, Cohen M. Dislocation theory of martensitic transformation. In: Nabarro FRN, editor. *Dislocations in Solids.* Amsterdam: North-Holland; 1986. p. 295–407.
39. Guimarães JRC, Rios PR. The constitution of martensite volume fraction in Fe-31wt%Ni-0.02wt%C. *J Mater Res Technol.* 2019;8(1):140-6.
40. Van Bohemen SMC, Sietsma J. Effect of composition on kinetics of athermal martensite formation in plain carbon steels. *Mater Sci Technol.* 2009;25(8):1009-12.
41. Maki T. Recent Advances in Understanding Martensite in Steels. In: Furuhashi T, Tsuzaki K, editors. *1st International Symposium on Steel Science; May 16-19 2007; Kyoto, Japan. Proceedings.* Tokyo; ISIJ; 2007. p. 1-10.
42. Rios PR, Villa E, de Oliveira SC. New methodology to model simultaneous and sequential reactions: main results and applications. *Mater Sci Forum.* 2012;706-709:149-56.
43. Rios PR, Villa E. On the Generalisation of JMAK's Theory. *Mater Sci Forum.* 2013;753:137-42.
44. Villa E, Rios PR. Transformation kinetics for nucleus clusters. *Acta Mater.* 2009;57(13):3714-24.
45. Villa E, Rios PR. Transformation kinetics for surface and bulk nucleation. *Acta Mater.* 2010;58(7):2752-68.
46. Borgenstam A, Hillert M. Activation energy for isothermal martensite in ferrous alloys. *Acta Mater.* 1997;45(2):651-62.
47. Villa M, Somers MAJ. Activation energy of time-dependent martensite formation in steel. In: Stebner A, Olson G, editors. *International Conference on Martensitic Transformations; 2018 Mai 13. Proceedings.* Chicago: Springer; 2018. p. 13–9.